Electro-optic and dielectric study of the de Vries–type smectic-A^* phase exhibiting transitions to smectic-C_A^* and smectic-C^* phases

U. Manna,[1] Jang-Kun Song,[1] Yu. P. Panarin,[1,2] Atsuo Fukuda,[1] and J. K. Vij[1,*]
[1]*Department of Electronic and Electrical Engineering, Trinity College, University of Dublin, Dublin 2, Ireland*
[2]*School of Electronic and Communication Engineering, Dublin Institute of Technology, Dublin 8, Ireland*
(Received 18 July 2007; revised manuscript received 9 February 2008; published 23 April 2008)

Mixtures of different compositions of an antiferroelectric liquid crystal compound that exhibits direct smectic-A^*(Sm-A^*)-smectic-C_A^*(Sm-C_A^*) transition with a ferroelectric liquid crystal compound that exhibits Sm-A^*-smectic-C^*(Sm-C^*) transition are studied using electro-optics and dielectric spectroscopy. The results of optical texture, birefringence, and the tilt angle suggest that a part of the Sm-A^* phase is of de Vries type, since an increase in the tilt angle with decreasing temperature results in a reduction in the value of the birefringence in the Sm-A^* phase, whereas the birefringence at Sm-A^* to Sm-C^* transition goes up by 12.7%. The soft mode relaxation strength, the Landau coefficient of the temperature dependent term, and the other related parameters of the de Vries–type Sm-A^*-Sm-C_A^* and Sm-A^*-Sm-C^* transitions are determined using the Landau theory of the second-order phase transition. For the Sm-A^*-Sm-C^* transition, we find that the soft mode relaxation strength decreases, the Landau coefficient increases, and the Curie-Weiss temperature range decreases with an increased ferroelectric composition in the mixture. These observations can be explained by assuming that with increased ferroelectric composition in the mixture, the layer shrinkage at the de Vries Sm-A^*-Sm-C^* transition increases. On comparing the results of de Vries–type Sm-A^* to Sm-C_A^* and Sm-C^* transitions, we find that the soft mode dielectric strength and the other related Landau parameters of the de Vries Sm-A^* phase are of the same order of magnitude for transitions from Sm-A^* to Sm-C^* and to Sm-C_A^* except for the composition of the mixture where both Sm-C^* and Sm-C_A^* transitions are stable and the phase diagram shows phase sequence Sm-A^* to Sm-C^* to Sm-C_A^*.

DOI: 10.1103/PhysRevE.77.041707 PACS number(s): 61.30.−v, 77.22.Gm, 77.80.Bh

I. INTRODUCTION

Liquid crystalline molecules are normally translationally anchored with an almost constant smectic layer spacing within the smectic-A^* (Sm-A^*) phase. At the transition from the Sm-A^* to smectic-C^* (Sm-C^*) or to smectic-C_A^* (Sm-C_A^*) phases, the director tilt that induces smectic layer spacing shrinkage starts at the transition into the Sm-C^* or Sm-C_A^* phase as shown in Fig. 1. This is normally the case except for some exceptional cases reported recently [1]. The layer shrinkage along with the surface anchoring of the molecules lead to the formation of chevrons. The chevrons of opposite fold directions are separated by zigzag defects which in turn degrade the quality of electro-optic devices based on ferroelectric liquid crystals (FLCs) [2,3] and antiferroelectric liquid crystals (AFLCs) [4,5]. As a result, the interest in zero or low layer shrinkage materials has increased significantly due to their potential use in displays and photonic devices [6]. The simplest structure of the Sm-A^* phase assumes that the smectic layer spacing (d_A) is equal to the molecular length L. If we assume perfectly ordered rodlike molecules with director tilt θ, the smectic layer spacing d_C is reduced to

$$d_C = d_A \cos\theta. \tag{1}$$

In the 1970s, x-ray experiments on smectic-A (Sm-A) phase of a number of achiral compounds carried out by Diele *et al.* [7], suggested that the smectic layer spacing d_A is 5%–10% lower than the calculated length L of the mesogenic molecules; this may lead to a constant layer spacing with decreasing temperature. Based on the experimental data by Diele *et al.*, de Vries suggested that both the Sm-A and smectic-C (Sm-C) phases are constituted of stacks of smectic layers where the molecules are tilted permanently and almost uniformly in each individual layer [8]. The direction of the local tilt fluctuations in the Sm-A phase are correlated at a short-range and this explains the absence of macroscopic tilt in the Sm-A phase, whereas in the Sm-C phase the tilt fluctuations are long-range correlated. As a result of the latter, the macroscopic tilt appears [9,10]. The possible directions of molecular fluctuations in the Sm-A phase are random and according to the de Vries scenario could occur on a diffuse cone, the cone angle of which is 2 times the average molecular inclination. The molecular arrangement becomes more ordered under decreasing temperature in Sm-A phase, or by increasing the electric field parallel to the smectic layers.

Recently several research groups [11–27] observed de Vries–type behavior in Sm-A^* phase using different techniques: X-ray diffraction, electro-optical techniques, dielectric, Raman and infrared spectroscopy. We recorded the optical texture, and measured the optical birefringence, and the tilt angle of an antiferroelectric liquid crystalline compound

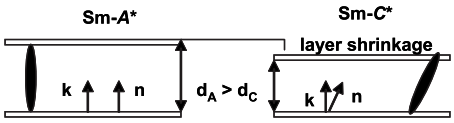

FIG. 1. Origin of the layer shrinkage at the Sm-A^*-Sm-C^* transition. At the transition from Sm-A^* to Sm-C^* phase, the director tilt induces a shrinkage in the smectic layer spacing starting at the transition into the Sm-C^* phase.

*Author to whom correspondence should be addressed; jvij@tcd.ie

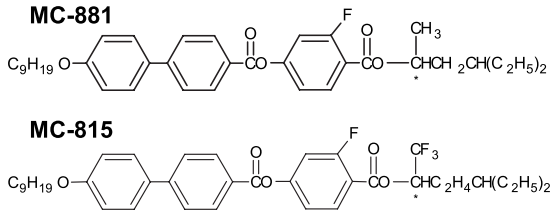

FIG. 2. Chemical structure of the compounds MC-881 and MC-815.

MC-881. Results of these measurements suggest that a part of Sm-A^* phase is of de Vries type, since an increase in the tilt angle coupled with a distribution of the directors with decreasing temperature results in a reduction in the birefringence in this phase. Different relaxation processes at the de Vries–type Sm-A^*-Sm-C_A^* transition were found from dielectric spectroscopic measurements. The relaxation frequency and the inverse of the soft mode dielectric relaxation strength of the de Vries–type Sm-A^* phase were plotted as a function of the temperature to calculate the different Landau parameters in de Vries–type Sm-A^* phase. Mixtures of MC-881 and different compositions of a FLC compound MC-815 were studied and the results suggest that a part of the Sm-A^* phase is of de Vries type in the mixtures too, since the birefringence at the Sm-A to Sm-C^* transition goes up by 12.7%. The soft mode strength and the different Landau parameters associated with de Vries–type Sm-A^*-Sm-C^* transition were calculated for different compositions of the mixtures to study the effect of the increased ferroelectric composition on the properties in Sm-A^* phase of the system exhibiting de Vries–type Sm-A^*-Sm-C^* transition. Results of de Vries Sm-A^* to Sm-C_A^* and to Sm-C^* transitions are also compared with the phase diagram of the ferroelectric and antiferroelectric liquid crystal mixtures.

II. EXPERIMENTAL RESULTS AND DISCUSSIONS

The chemical structure of the AFLC compound MC-881 and FLC compound MC-815 [28,29], used for experiments are shown in Fig. 2. For optical texture and the tilt angle measurements, each of the cells of 9 μm thickness with planar alignment are filled with the AFLC compound MC-881 and different compositions of the mixtures of MC-881 and MC-815. The phase sequence and the order of the transitions of the phases of both compounds and their mixtures are shown in Table I. Note that the Sm-A^*-Sm-C^* transition temperature decreases with increased ferroelectric composition in mixtures. The cells were made of two chemically etched indium tin oxide (ITO) coated glass plates with sheet resistance of 30 $\Omega/\square$. For planar alignment, the conducting inner surfaces were spin coated with a polyimide RN 1175 alignment layer and rubbed parallel. The cells are filled with liquid crystals in the isotropic state and then cooled down slowly from 125 °C. The cells were kept in a hot stage, the temperature of which was controlled by Eurotherm-2604 temperature controller with an accuracy better than 10 mK. The hot stage was mounted on the rotating table of an Olympus microscope. The apparent tilt angle (θ_A) was measured by applying a low frequency field and rotating the sample by rotating the stage on which it is mounted in the polarizing microscope from the dark to the bright state. The birefringence measurements were based on the spectral measurement of the light transmitted through the liquid crystal cell placed between the crossed polarizers [19,22]. The transmitted light was coupled into a fiber optic and routed to a AVASPEC 2024 spectrometer in turn connected to a PC where the spectrum was processed. Dielectric measurements in the frequency range ranging from 1 Hz to 10 MHz were carried out by using the Novocontrol Alpha High Resolution Dielectric Analyzer. During dielectric measurements, the system allowed us to superimpose dc bias voltages up to 40 V on an ac voltage rms of 0.03 V.

A. Electro-optics of de Vries–type Sm-A^* phase that exhibits Sm-C_A^* and Sm-C^* transitions

1. Optical texture study of the antiferroelectric compound MC-881 in the Sm-A^* *phase*

The optical textures were recorded to study the properties of Sm-A^* phase in MC-881. Figure 3(a) shows the geometry

TABLE I. Phase sequence and the order of the transitions of the phases of MC-881 and MC-815 and their mixtures.

MC-881	Sm-C_A^*	$\frac{1st}{112.5\ °C}$	Sm-A^*	$\frac{1st}{120\ °C}$	I
MC-815	Sm-C^*	$\frac{1st}{96\ °C}$	I		
Mixture-1 (12% MC-815 +88% MC-881)	Sm-C^*	$\frac{2nd}{110.5\ °C}$	Sm-A^*	$\frac{1st}{120\ °C}$	I
Mixture-2 (20% MC-815 +80% MC-881)	Sm-C^*	$\frac{2nd}{110\ °C}$	Sm-A^*	$\frac{1st}{120\ °C}$	I
Mixture-3 (28% MC-815 +72% MC-881)	Sm-C^*	$\frac{2nd}{108\ °C}$	Sm-A^*	$\frac{1st}{120\ °C}$	I

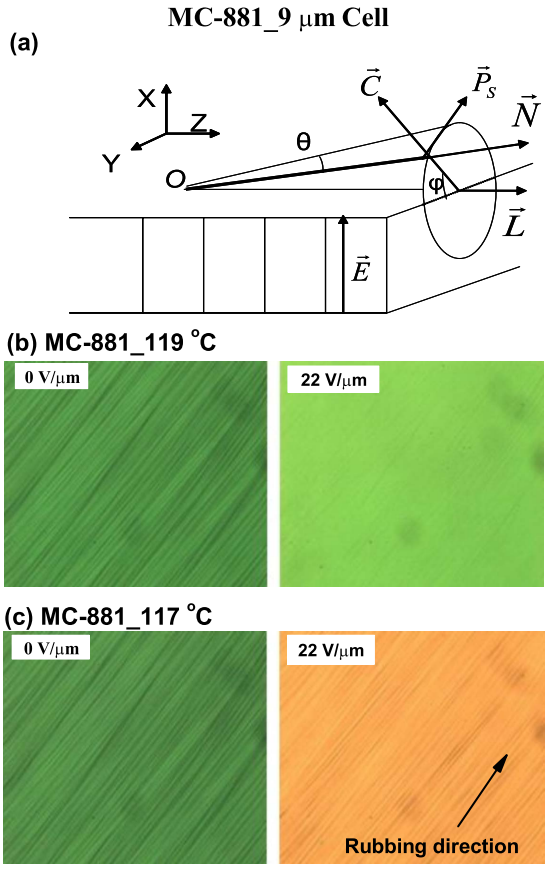

FIG. 3. (Color online) (a) The geometry of the studied sample. Planar texture of MC-881 at 119 °C (b) and 117 °C (c) with and without applied voltage. At 119 °C, application of the external electric field yields only a change in the transmitted light intensity while the color of the texture remains about the same. At 117 °C, application of the external electric field produces a change in the birefringence, confirming the existence of the de Vries–type Sm-A^* phase.

of the studied sample; (X,Y,Z) are the orthogonal axes of the coordinate system, N is the molecular director, L is the smectic layer normal, C is the c director, θ is the tilt angle, and φ is the azimuthal angle; the plane YZ is that of the glass plate. Figures 3(b) and 3(c) show the textures for planar cells taken at two different temperatures: 119 °C and 117 °C, respectively, after having applied electric field to obtain better alignment during cooling of the sample from the isotropic phase. When placed between the two crossed polarizers, the planar cell filled with the AFLC compound in the Sm-A^* phase at 119 °C shows a uniform dark green color due to a finite birefringence. The application of an electric field parallel to the smectic layer induces a molecular tilt with the same symmetry as Sm-C^*. However this does not change the birefringence but only the intensity of light. As a result, there is only a change in the transmitted light intensity while the color of the texture remains almost the same. Conversely, at a lower temperature of 117 °C, the cell shows different behavior. The application of an external electric field produces a significant change in the color of the planar texture as shown in Fig. 3(c). This can be explained in terms of the de Vries scenario of the diffuse cone model. In the de Vries Sm-A^* phase, the molecules though significantly tilted are also azimuthally disordered. The external electric field produces a bias in the distribution of the tilt directions with the same symmetry as Sm-C^* through an azimuthal ordering of the already tilted molecules. This results in a significantly better alignment and a change in the birefringence and therefore a change in the spectrum of the transmitted light, and hence a change in the color of the planar texture.

The stripe texture is observed in Figs. 3(b) and 3(c) at both temperatures parallel to the rubbing direction. We suggest that these stripes are induced first at 119 °C by the electric field applied parallel to the smectic layers. These stripes possibly arise from a reduction in the smectic layer spacing due to the molecular tilting by the electroclinic effect and a consequent smectic layer buckling induced by the electric field [30–32]. These stripes are rather stable and continue persisting even after the electric field is turned off in the Sm-A^* phase [30] and even in the Sm-C^* phase [33]. As observed in our experiments these stripes persist even when the sample is cooled down to Sm-C_A^* phase. This makes it almost impossible to compare a change in the stripe textures in the conventional and de Vries–type Sm-A^* phases as observed in our case.

2. Birefringence and tilt angle of the antiferroelectric compound MC-881 exhibiting Sm-A^* *to* Sm-C_A^* *transition based on spectral measurement of light*

As mentioned above de Vries materials show a large variation in the birefringence with electric field and therefore the optical spectra under an applied electric field changes. As the color changes, the spectrum peak moves to a different wavelength within the range of visible light. This property can be used to determine the optical birefringence (Δn) and the molecular tilt angle (de Vries tilt angle, θ_{dV}) in the uniaxial Sm-A^* phase [19,22]. The light transmitted through the cell placed in between the crossed polarizers as a function of the wavelength is given as

$$T = A \sin^2\left(\frac{\pi \Delta n_{\mathrm{eff}} d}{\lambda}\right) + B. \tag{2}$$

Here A is a scaling factor that depends on the orientation of the optical axis of the cell with respect to the polarizer and the intensity of the light source, d is the cell thickness, λ is the wavelength of light, Δn_{eff} is the effective birefringence, and B is an offset signal. Through a fitting of the transmittance spectra for each field, it is possible to obtain the birefringence as a function of the applied field. To ensure a proper fitting of the spectra, we must consider the dependence of Δn on wavelength. The extended Cauchy equation [34]. was used for the fitting of the data on the transmitted intensity as a function of the wavelength,

$$\Delta n_{\mathrm{eff}}(\lambda) = k_{\mathrm{eff}}\left(\frac{\lambda^2 \lambda^{*2}}{\lambda^2 - \lambda^{*2}}\right). \tag{3}$$

The parameters k_{eff} and λ^* were determined from fitting the optical spectrum at a large enough electric field at which the molecules of the de Vries structure are confined to $\varphi = 0$ on the smectic cone and $\cos\varphi \approx 1$ and $\cos^2\varphi \approx 1$ and the effec-

tive birefringence $[\Delta n \equiv \Delta n_{\text{eff}}(E_{\text{high}})]$ is maximal, where φ denotes the azimuthal angle as shown in Fig. 3(a). In the absence of the electric field the effective birefringence of the de Vries phase (Δn_0) is always lower than Δn, but the dispersion is the same. Therefore, during the fitting of the optical spectra in the absence of the electric field, the dispersion parameter λ^* was fixed and the only fitting parameter was the scaling factor k_{eff}. From a comparison of the values of the birefringence in the undisturbed de Vries phase (without applied field) (Δn_0) and saturated birefringence (with applied field) (Δn), we may estimate the tilt angle of the de Vries phase using the expression [15]

$$\frac{\Delta n_0}{\Delta n} \equiv \frac{k_0}{k} = 1 - \frac{3}{2}\sin^2 \theta_{\text{dV}}, \tag{4}$$

where $k_{\text{eff}}=k_0$ in the absence of the electric field and $k_{\text{eff}}=k$ in the presence of the electric field are obtained from the fitting of the spectra for zero and high values of the electric field, respectively. Finally, we can easily determine the de Vries tilt angle θ_{dV} by using the following algebraic equation based on Eq. (4):

$$\theta_{\text{dV}} = \arcsin\sqrt{\frac{2}{3}\left(1 - \frac{k_0}{k}\right)}. \tag{5}$$

Figure 4(a) shows the results of the birefringence measurement with and without applied field. On cooling the sample from the isotropic phase to the Sm-A^* phase, in the absence of the electric field, the birefringence increases as expected, but then saturates and finally decreases within the Sm-A^* phase itself as shown in the inset of Fig. 4(a). On further cooling the sample from the Sm-A^* phase to the Sm-C_A^* phase, in the absence of the electric field, the birefringence goes down drastically near an apparent transition and then continues to decrease slowly with decreasing temperature. The same measurements with applied field ($E = 22.22$ V/μm) show a continuous growth of the birefringence in the entire range of temperatures corresponding to the Sm-A^* phase and the Sm-C_A^* phase. The birefringence is determined by the molecular distribution of the material in a phase confined within the cell. In the uniaxial Sm-A^* phase, the birefringence can be expressed as [35]

$$\Delta n = n_e - n_0 = \frac{N}{3\epsilon_o}\left(\frac{n^2+2}{n_e+n_0}\right)(\Delta\alpha S), \tag{6}$$

n_e and n_o are the extraordinary and the ordinary refractive indices, N is the molecular number density, n is the refractive index, ϵ_0 is the permittivity of free space, $\Delta\alpha \equiv \alpha_z - (\alpha_x + \alpha_y)/2$ is the polarizability anisotropy, and S is the orientational order parameter. Equation (6) suggests that $\Delta n \propto S$. Thus, a change in the orientational order parameter S can easily be detected by a change in the birefringence. Even in the biaxial phases, the biaxiality is usually much smaller than the birefringence, and Eq. (6) is approximately valid. In the transition from de Vries–type Sm-A^* to Sm-C_A^*, the orientational order parameter may always show a sudden decrease in the value and this is independent of the random distribution of directors because of their anticlinic arrangement between the neighboring layers in Sm-C_A^*. In the temperature

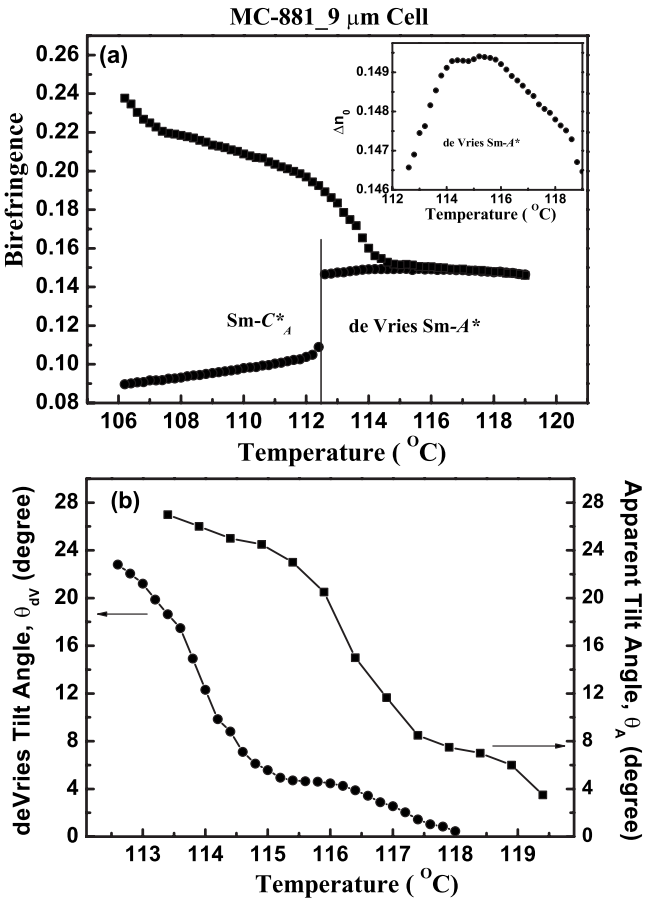

FIG. 4. (a) Temperature dependence of the birefringence for $\lambda = 550$ nm with (■) and without (●) voltage in the Sm-A^* phase and Sm-C_A^* phase. The inset in the figure shows the temperature dependence of the birefringence only within the Sm-A^* phase without voltage. (b) Temperature dependence of the tilt angle in the Sm-A^* phase for MC-881. The results confirm the existence of the de Vries–type Sm-A^* phase within the Sm-A^* phase.

range corresponding to the conventional Sm-A^* phase, the birefringence increases with decreasing temperature due to an increase in the orientational order parameter. In the temperature range corresponding to the de Vries–type Sm-A^* phase, the macroscopic order parameter, measured by the birefringence is lower than in the conventional Sm-A^* phase due to a molecular tilt and a distribution of the azimuthal angle. The disorder in the azimuthal angle with a tilt results in a reduction in the value of the birefringence with decreasing temperature. An application of the electric field in the de Vries–type Sm-A^* phase, forces these molecules to align in the same direction in the tilt plane normal to the electric field. This increases the birefringence; whereas in the conventional Sm-A^* phase, an application of the electric field induces only an in-plane tilt of the in-layer director, birefringence remains the same in the presence or absence of the field. However, both the conventional Sm-A^* phase and de Vries–type Sm-A^* phase possess uniaxial symmetry, there is no distinct step in the birefringence, rather there is a continuous change in it. Hence it may be difficult to determine the transition temperature precisely. The crossover point between the conventional Sm-A^* phase and de Vries–type

Sm-A^* phase was determined by observing a change in the color of the planar texture with the application of a maximum available external voltage (200 V) corresponding to a field of 22.22 V/μm. It is necessary to mention that the crossover point moves to lower temperatures with a decrease in the applied voltage. Therefore, we can anticipate that it will move to higher temperatures by applying higher voltages. This means that the threshold field at which the de Vries structure starts to change depends strongly on the temperature. Therefore, a crossover point is not the transition temperature between the de Vries–type Sm-A^* and the conventional Sm-A^*. It may correspond to phase transition only when a sufficiently large electric field is applied, which is not the case in our experiment, thus we cannot determine the phase transition temperature. Moreover, we cannot state with certainty whether or not such a transition exists in the sample. The temperature dependence of the de Vries tilt angle, θ_{dV} calculated by using Eq. (5) and the apparent tilt angle (θ_A) are plotted in Fig. 4(b). In a conventional Sm-A^* phase, the measured (apparent) tilt angle (θ_A) is mainly due to the electroclinic effect, $\theta_A = \theta_E$. In the de Vries–type Sm-A^* phase, the apparent tilt angle is due to the biasing of the molecular azimuthal distribution in the direction perpendicular to the electric field which is in addition to that caused by the electroclinic effect. Hence at a sufficiently large electric field, the apparent tilt angle must be saturated if the contribution of the electroclinic effect is small. In practice, however, the apparent tilt angle continues to grow slightly with an increase in the electric field arising mainly from the conventional electroclinic effect [21]. In de Vries–type Sm-A^* phase, we thus have $\theta_A = \theta_{\mathrm{dV}} + \theta_E$, where θ_{dV} is the de Vries tilt angle (thermodynamical tilt angle) and θ_E is the induced tilt angle (electroclinic tilt angle). A parameter (tiltness) is introduced to measure the de Vries properties of Sm-A^* materials: $t_A = \theta_{\mathrm{dV}}/\theta_A$. For conventional Sm-$A^*$ compounds, $t_A = 0$, while for ideal de Vries materials, $t_A = 1$. For MC-881, at the temperature just above the de Vries–type Sm-A^* to Sm-C_A^* (or Sm-C^*) phase transition, we found $t_A = \theta_{\mathrm{dV}}/\theta_A = 18.63/27 = 0.69$.

3. Birefringence and tilt angle measurements of the antiferroelectric and ferroelectric liquid crystal mixtures exhibiting Sm-A^* *to* Sm-C^* *transition based on the spectral measurement of light*

We studied different mixtures of the antiferroelectric MC-881 and the ferroelectric MC-815 liquid crystalline compounds with an increased composition of MC-815 in the mixture. The compositions and the phase sequences of the mixtures are shown in Table I. The mixtures exhibit the direct de Vries–type Sm-A^*-Sm-C^* transition rather than de Vries–type Sm-A^*-Sm-C_A^* transition as in the pure antiferroelectric liquid crystalline compound MC-881. The mixtures provide us with a possibility of studying an effect of the increased ferroelectric composition on the properties of de Vries–type Sm-A^* phase at de Vries–type Sm-A^*-Sm-C^* transition. The birefringence and the tilt angle measurements based on the spectral measurements of the light transmitted through the liquid crystal were carried out for the various mixtures and the optical textures recorded. The experimental results for the Mixture-2 are shown in Fig. 5. Figures 5(a)–5(c) show the optical textures of the Sm-A^* and Sm-C^* phases on cooling the sample from the isotropic phase. Figure 5(d) shows the birefringence measurement with and without the applied field. On cooling the cell from the isotropic to the Sm-A^* phase, in the absence of the electric field,

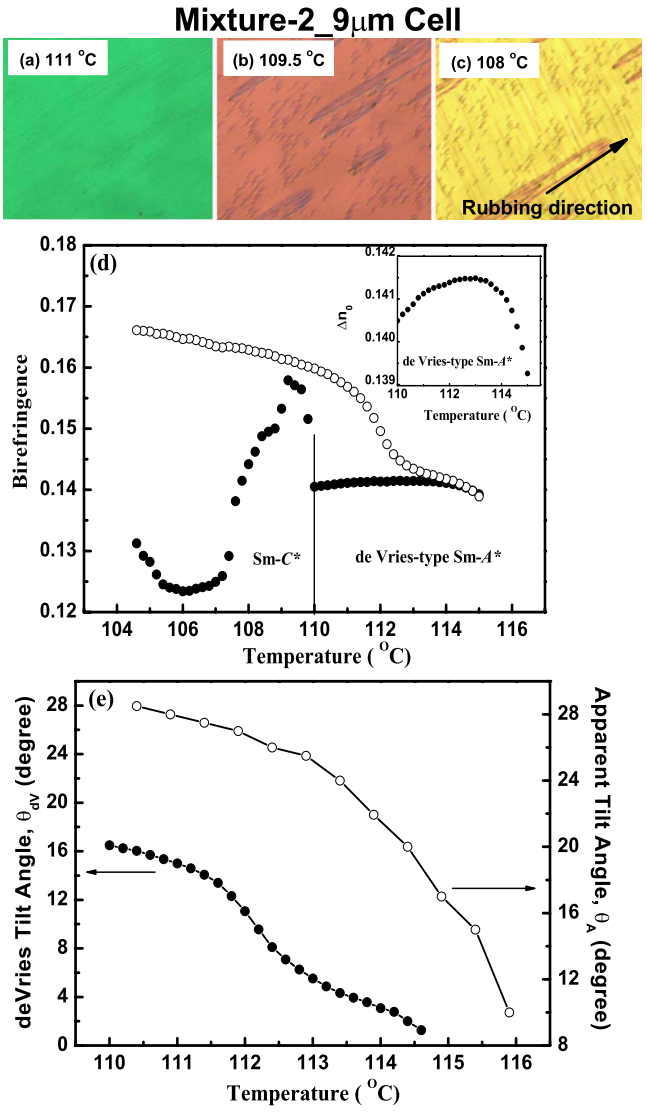

FIG. 5. (Color online) Optical textures of Sm-A^* phase at 111 °C (a), Sm-C^* phase at 109.5 °C (b), and the Sm-C^* phase at 109 °C (c). In the Sm-C^* phase at 108 °C (c), one observes the disclination lines, appearing due to the helical structure. The arrow in (c) represents the rubbing direction. The domain boundaries due to the surface-stabilized state appear along the rubbing direction, whereas, the disclination lines due to the helical structure appear perpendicular to the rubbing direction. But in the Sm-C^* phase at 109.5 °C (b), there is no such line. (d) The temperature dependence of the birefringence in the Sm-A^* and Sm-C^* phases with (○) and without (●) voltage. The inset in the figure shows the temperature dependence of the birefringence only within the Sm-A^* phase without voltage. (e) The temperature dependence of the tilt angle in Sm-A^* phase for Mixture-2. The results confirm the existence of de Vries–type Sm-A^* phase in the mixture. Birefringence data are plotted for $\lambda = 550$ nm.

the birefringence increases as expected, but then saturates and finally decreases within the Sm-A^* phase as shown in the inset in Fig. 5(d), as in the case of pure AFLC, MC-881. But, on further cooling the sample from Sm-A^* to the Sm-C^* phase, again in the absence of the electric field, the birefringence goes up approximately 12.7% near the transition temperature and then continues to decrease slowly with decreasing temperature. This is quite different from what is normally expected from a conventional Sm-A^*-Sm-C^* transition. In which case the spatial averaging of the optical properties, resulting from the helix formation, decreases the birefringence in the helical state. In the surface-stabilized state however, for a conventional Sm-A^*-Sm-C^* transition, one may expect a small increase in the birefringence due to the transition from a uniaxial state to a biaxial state, but the magnitude of this change is rather too small. On the other hand, the observed behavior can be very well explained by a de Vries–type Sm-A^*-Sm-C^* transition. In the transition from de Vries Sm-A^* to Sm-C^*, if the helical structure is suppressed by the surface anchoring, which is usually the case in planar cells, S order parameter may show a sudden increase because the randomly distributed liquid crystalline molecules in de Vries Sm-A^* phase align along the same direction as in the Sm-C^* phase. However, if the helical structure is not suppressed, S may decrease. If Sm-A^* phase is not a de Vries phase but a conventional Sm-A^* phase, S may not show any sudden change at the transition, but show a little change or a slow decrease. This explanation is confirmed by the optical textures shown in Figs. 5(a)–5(c), where at the transition from Sm-A^* phase (a) to the Sm-C^* phase at 108 °C (c), one can see the appearance of disclination lines due to the appearance of the helical structure. The arrow in Fig. 5(c) represents the rubbing direction. The domain boundaries due to the surface-stabilized state appear along the rubbing direction, whereas, the disclination lines due to the helical structure appear perpendicular to the rubbing direction. But in the Sm-C^* phase at 109.5 °C (b), there are no such lines. The birefringence measurement with applied field (E=22.22 V/μm) show a continuous growth of the birefringence in the entire temperature range corresponding to the Sm-A^* phase and the Sm-C_A^* phase, as in the case of pure AFLC, MC-881. This confirms the existence of a tilted de Vries–type Sm-A^* phase in Mixture-2. The temperature dependence of the de Vries tilt angle, θ_{dV} calculated by using Eq. (5) and the apparent tilt angle (θ_A) are plotted in Fig. 5(e). The tiltness of the de Vries–type Sm-A^* materials at the temperature just above the de Vries–type Sm-A^* to Sm-C_A^* (or Sm-C^*) phase transitions, is supposed to be $t_A=\theta_{\mathrm{dV}}/\theta_A=16.03/28.50=0.56$.

B. Dielectric study of the de Vries–type Sm-A^*-Sm-C_A^* transition

1. Soft-mode fluctuations

Figure 6 shows the dependence of the dielectric relaxation strength ($\Delta\epsilon$) and the relaxation frequency (f_R) on temperature of the compound MC-881 for a 20 μm cell without applying any dc-bias voltage such that $f_R=f_{\max}=1/2\pi\tau_j$, where $f_{\max}$ is the frequency for which ϵ'' is maximum. The $\Delta\epsilon$ and f_R are found by fitting the dielectric spectra to the

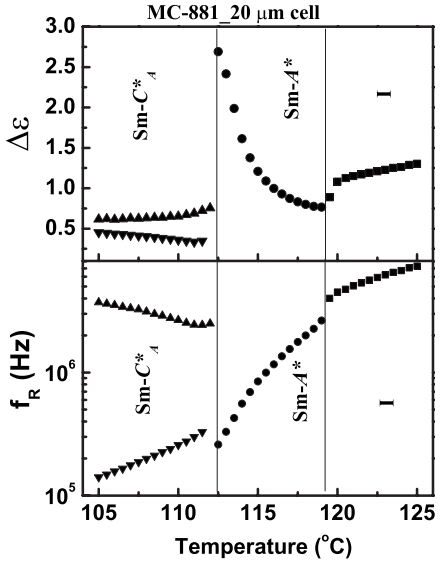

FIG. 6. Dependence of the dielectric relaxation strength ($\Delta\epsilon$) spectra and the relaxation frequency (f_R) on temperature of MC-881 for 20 μm cell thickness. The collective mode appearing around the de Vries–type Sm-A^*-Sm-C_A^* transition corresponds to the fluctuations of the tilt angle of the director.

Havriliak-Negami equation using WINFIT fitting program. The Havriliak-Negami equation for n relaxation processes is given by

$$\epsilon^*(\omega)=\epsilon'-i\epsilon''=\epsilon_\infty+\sum_{j=1}^{n}\frac{\Delta\epsilon_j}{[1+(i\omega\tau_j)^\alpha]^\beta}, \tag{7}$$

where ϵ_∞ is the high-frequency permittivity, j is a variable denoting the number of the relaxation processes up to n. τ_j is the relaxation time and $\Delta\epsilon_j$ is the dielectric relaxation strength of jth relaxation process, respectively. α and β are the fitting parameters for the jth process. In the temperature range corresponding to the de Vries–type Sm-A^* phase, only one relaxation mode (the soft mode), corresponding to the fluctuations of the primary order parameter, the tilt angle, is detected. Whereas, in the Sm-C_A^* phase two relaxation modes are detected [36]. We will restrict ourselves to the considerations of the soft mode as we are interested mainly in the fluctuations of the tilt angle in the de Vries–type Sm-A^* phase. Sometimes there may be some differences in the soft mode fluctuations of the conventional and de Vries–type materials. Since fluctuations of the director tilt angle, in the Sm-A^* and Sm-C^* are coupled to the variations in the magnitude of the polarization, these appear as a pronounced soft mode absorption [37]. Remarkably strong soft mode absorption is also found in the dielectric spectra of some de Vries materials in comparison to the materials [20] that exhibit a conventional Sm-A^* phase.

2. Landau parameters

The generalized Landau expansion of Sm-A^*-Sm-C^* transition, where the nonsingular part of the free energy $f-f_0$ in the vicinity of the Sm-A^*-Sm-C^* transition is given by a power series expansion in terms of the primary (Θ) and sec-

ondary (P) order parameters, proposed by Žekš in 1984 [38], is given by

$$f - f_0 = \frac{1}{2}\alpha(T - T_c)\Theta^2 + \frac{1}{4}b\Theta^4 + \frac{1}{6}c\Theta^6 - CP\Theta + \frac{1}{2\chi\epsilon_0}P^2 - \frac{1}{2}\Omega P^2\Theta^2 + \frac{1}{4}\eta P^4 - PE. \quad (8)$$

The first three terms represent the free energy of the Sm-C^* phase with Landau coefficients α, b, and c. The polarization-tilt coupling is reflected in the bilinear $(-CP\Theta)$ and biquadratic $(-\Omega P^2\Theta^2/2)$ coupling terms, introducing the coefficients C and Ω. The $P^2/2\chi\epsilon_0$ term is entropic in origin, related to a decrease in the entropy due to the polar ordering in the material. The last term describes the contribution due to a nonzero electric field. The individual properties of a certain ferroelectric material are reflected by its Landau expansion coefficients, i.e., α, b, c, C, χ, and Ω in the above equation.

The temperature dependence of the soft-mode relaxation frequency and the dielectric strength in the Sm-A^* phase on approaching the Sm-A^*-Sm-C^* transition can be calculated from the above free energy expression as [39]

$$f_R = \frac{\alpha(T - T_c)}{2\pi\gamma}, \quad T > T_c, \quad (9)$$

$$\Delta\epsilon_s = \frac{\epsilon_0(\chi_f C_f)^2}{\alpha(T - T_c)}, \quad T > T_c, \quad (10)$$

where f_R and $\Delta\epsilon_s$ are the relaxation frequency and the dielectric strength of the soft mode, α is the Landau coefficient of the temperature-dependent term in the free energy expression, γ is the viscosity connected with the soft mode, assumed to be temperature independent, ϵ_o is the permittivity of free space, χ_f is the susceptibility of the ferroelectric amplitude mode, C_f is the coupling constant between the polarization and the tilt angle of the ferroelectric amplitude mode, T_c is the transition temperature of Sm-A^*-Sm-C^* transition, defined as the frequency for which $1/\Delta\epsilon_s$ is a minimum. Equation (10) shows that in the Sm-A^* phase, the inverse of the dielectric strength $(1/\Delta\epsilon_s)$ varies linearly with temperature, called the Curie-Weiss (CW) law. According to Žekš and Čepič [40], we may expect two amplitude modes in Sm-A^* phase, one ferroelectric and a second antiferroelectric. The antiferroelectric mode does not contribute to the dielectric permittivity and therefore we can neglect it. Frequencies of two amplitude modes tend to zero (softening) at different temperatures. If the ferroelectric amplitude mode condenses at higher temperature than the antiferroelectric amplitude mode $(T_f > T_a)$, the Sm-A^*-Sm-C^* phase transition occurs. If the reverse is true $(T_f < T_a)$, the Sm-A^*-Sm-C_A^* transition occurs. The dielectric response in the Sm-A^* phase exhibiting Sm-C_A^* transition should be similar to the dielectric response of the Sm-A^* phase exhibiting Sm-C^* transition as the equations describing the electroclinic effect (linear coupling of the electric field to the ferroelectric order parameter) and the dynamics of the ferroelectric amplitude mode are the same [41–43]. We apply the Landau theory of the dielectric response of the conventional second-order Sm-A^*-Sm-C^* transition to de Vries–type Sm-A^*-Sm-C_A^* transition to determine the Landau parameters associated with the de Vries–type Sm-A^*-Sm-C_A^* transition.

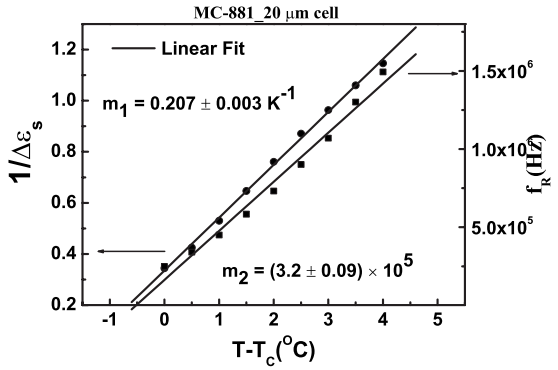

FIG. 7. Temperature dependence of the relaxation frequency and the inverse of the soft mode relaxation strength in the de Vries–type Sm-A^* phase in MC-881.

The linear electroclinic response to the applied field in the paraelectric Sm-A^* phase can be written as $\theta = eE$, Where the e is the electroclinic coefficient, given by [44]

$$e = \frac{\epsilon_0\chi_f C_f}{\alpha(T - T_c)}. \quad (11)$$

Figure 7 shows the temperature dependence of the relaxation frequency (f_R) and the inverse of the soft mode relaxation strength $(1/\Delta\epsilon_s)$ in de Vries–type Sm-A^* phase for 20 μm cell thickness. The slope of the temperature dependence of f_R and $1/\Delta\epsilon_s$ are also calculated to find different Landau param-

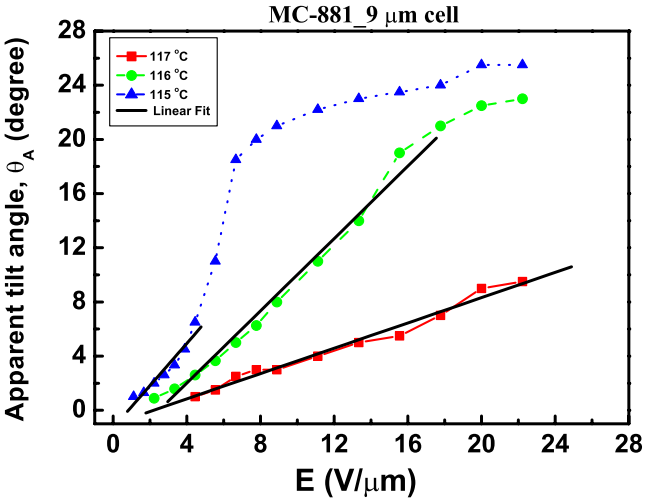

FIG. 8. (Color online) Apparent tilt angle as a function of the applied field at different temperatures for the cell thickness of 9 μm. In the de Vries–type Sm-A^* phase linear regime is observed for low values of the measuring field. Results for the tilt angle dependence on the electric field are reminiscent of the devil staircase observed similarly in the Sm-C_α^* phase of 4-(1-metylheptyloxycarbonyl) phenyl 4′ -octyloxy- biphenyl-4-carboxylate (MHPOBC) by Hiraoka *et al.*, their Fig. 3 (curves b and c) [49].

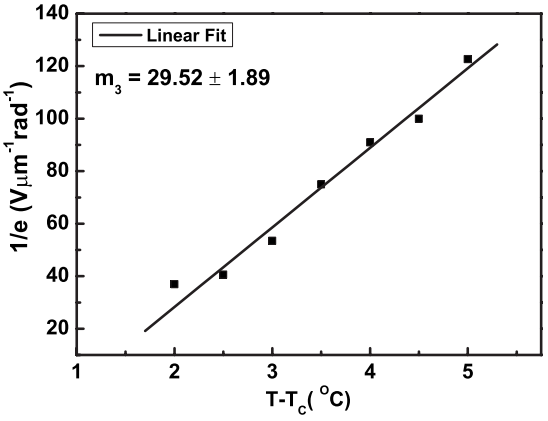

FIG. 9. Inverse electroclinic coefficient as a function of temperature of MC881.

eters at the de Vries–type Sm-A^*-Sm-C_A^* transition. Figure 8 shows the dependence of the apparent tilt angle as a function of the applied field at different temperatures for a cell of thickness 9 μm. A strong increase in the dielectric amplitude of the soft mode, when approaching de Vries–type Sm-A^*-Sm-C_A^* transition, indicates a tilt induced by the field. At a lower temperature in the de Vries–type Sm-A^* phase, a strong electric field induces an apparent tilt angle that can nearly be of the same order as the saturation tilt angle in the Sm-C_A^* phase. For low values of E, the tilt angle varies linearly with the electric field in the de Vries–type Sm-A^* phase. Above a certain value of the field, the linear relation is no longer valid and at this stage a transition from de Vries–type Sm-A^* phase to a ferroelectric state is possible. Figure 8 also suggests that the field dependence of the apparent tilt angle in de Vries–type phase Sm-A^* is changing from Langevin type in Sm-A^* phase at 117 °C to a discontinuous one at 115 °C. The electronic coefficient e has been determined from the linear part of the $\theta(E)$ curves. The temperature dependence of the reciprocal value of the electroclinic coefficient $1/e$ in de Vries–type Sm-A^* phase is shown in Fig. 9. In the studied temperature range above T_c, the temperature dependencies of the quantities characterizing the soft mode of de Vries–type Sm-A^* phase; $1/\Delta\epsilon_s$, f_R, and $1/e$, shown in Figs. 7 and 9 confirm the simple linear description given by the expressions in Eqs. (9)–(11). From slopes of those dependencies and using Eqs. (9)–(11) the Landau parameters α, $\chi_f C_f$, γ are calculated and given in Table II.

TABLE II. Numerical results obtained by fitting the theoretical expressions for MC-881 for a cell thickness of 20 μm.

$\chi_f C_f = (1.44 \pm 0.09) \times 10^8$ V m^{-1} rad^{-1}
$\alpha = (38 \pm 2.59)$ kN m^{-2} rad^{-2} K^{-1}
$\gamma = (1.9 \pm 0.18) \times 10^{-2}$ Pa s

With an exception of the viscosity coefficient, γ, which is very low, different Landau parameters for de Vries–type Sm-A^*-Sm-C_A^* transition are found to be of the same order of magnitude to those obtained for a conventional Sm-A^*-Sm-C_A^* transition [41].

C. Dielectric study of the Sm-A^*-Sm-C^* transition in different mixtures of MC-815 and MC-881

1. Soft mode fluctuations

Dielectric measurements were carried out for three mixtures: 1, 2, and 3 with and without dc-bias field applied across a 20 μm planar cell. As the mixtures exhibit de Vries–type Sm-A^*-Sm-C^* transition, the soft mode is made visible by applying an external dc-bias field since suppression of the Goldstone absorption by dc bias is far more effective than the suppression of the soft mode [45]. Figure 10 shows the dependence of the real part of relative dielectric permittivity spectra (ϵ') of the three mixtures: 1, 2, and 3, on temperature for a 20 μm cell under an applied dc bias of 2 V/μm. The dielectric loss spectra with and without applied dc bias for the various mixtures are fitted to the Havriliak-Negami equation [Eq. (7)] to find $\Delta\epsilon$ at the de Vries–type Sm-A^*-Sm-C^* transition. Figure 11(a) shows the dependence of $\Delta\epsilon$ on temperature without applied dc bias for mixtures 1, 2, and 3. We note that $\Delta\epsilon$ without application of dc bias at de Vries–type Sm-A^*-Sm-C^* transition goes up with increased ferroelectric composition in the mixtures as the Goldstone mode becomes gradually stronger in the mixture [46]. But the experimental observations become interesting when the Goldstone mode is suppressed by applying the dc bias. With the application of the dc bias, only the soft mode is visible at the de Vries–type Sm-A^*-Sm-C^* transition

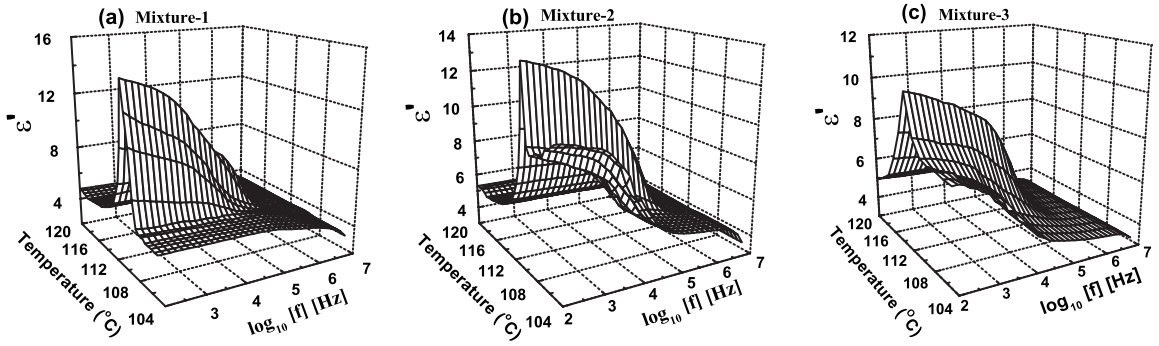

FIG. 10. Dependence of the dielectric loss spectra (ϵ') on temperature and frequency of (a) Mixture-1, (b) Mixture-2, and (c) Mixture-3 under applied dc bias of 2 V/μm for 20μm cell. DC bias of 2 V/μm is applied to suppress the Goldstone mode at de Vries–type Sm-A^*-Sm-C^* transition.

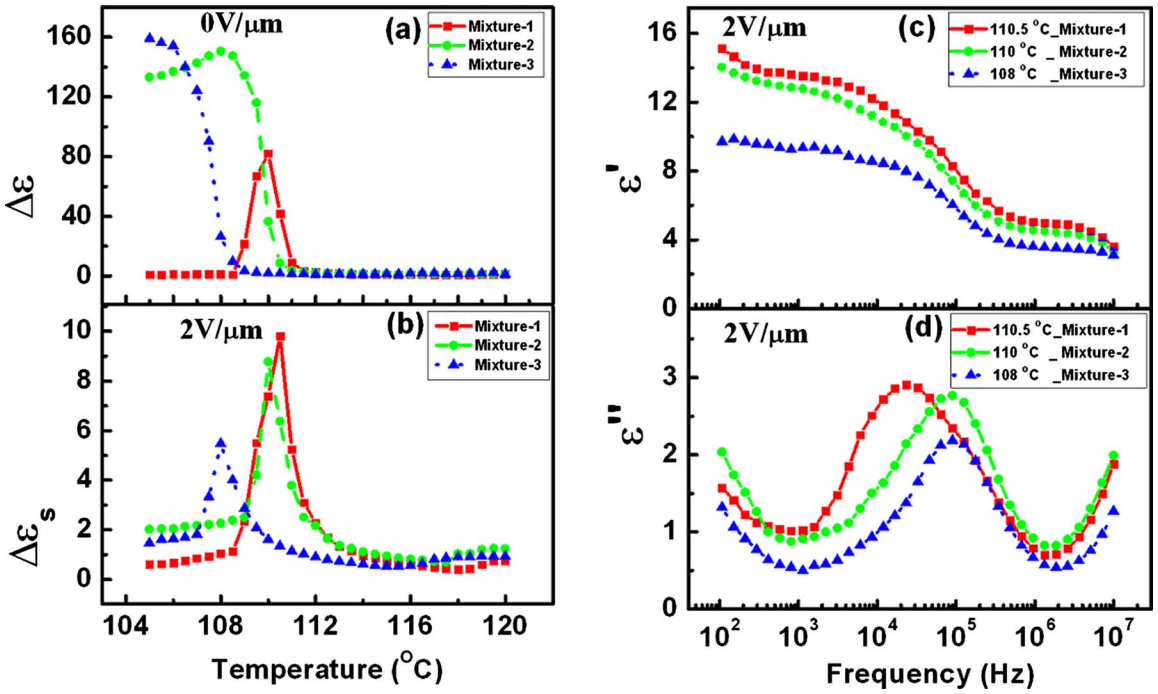

FIG. 11. (Color online) Dependence of the dielectric relaxation strength without (a) and with (b) dc bias on temperature for different compositions of MC-815 and MC-881 mixtures in 20 μm cell and the real (c) and the imaginary (d) parts of the dielectric permittivity with dc bias at de Vries–type Sm-A^*-Sm-C^* transition temperatures of different compositions of MC-815 and MC-881 mixture for 20 μm cell thickness.

and we see that the soft mode strength ($\Delta\epsilon_s$) at the de Vries–type Sm-A^*-Sm-C^* transition temperature goes down by increasing ferroelectric composition in the mixture as shown in Fig. 11(b). The spectra of the real (ϵ') and imaginary parts (ϵ'') of the dielectric permittivity for all the mixtures at the de Vries–type Sm-A^*-Sm-C^* transition temperature with applied dc bias are plotted as a function of frequency in Figs. 11(c) and 11(d), respectively. We observe that the amplitudes of ϵ' and ϵ'' with application of dc bias go down with increasing ferroelectric composition in the mixture at the de Vries–type Sm-A^*-Sm-C^* transition temperature. The values of the soft mode dielectric strength ($\Delta\epsilon_s$) at the Sm-A^*-Sm-C^* transition for different mixtures are listed in Table III.

2. Landau parameters

The amplitude mode in de Vries–type Sm-A^* phase exhibiting Sm-C^* transition can be described by Eqs. (9) and (10). The Curie-Weiss plot of the inverse dielectric strength ($1/\Delta\epsilon_s$) as a function of the difference between the measured temperature and transition temperature, Curie point $T-T_c$ for the three mixtures without application of bias field is shown in Fig. 12. This shows a Curie-Weiss plot at de Vries–type Sm-A^*-Sm-C^* transition for a 20 μm cell. From the linear fits of f_R and $1/\Delta\epsilon_s$ as a function of a difference in the temperature from the transition temperature and the plots of the apparent tilt angle as a function of the applied field in de Vries–type Sm-A^* phase of all three mixtures, we can calculate the different Landau parameters for de Vries–type Sm-A^*-Sm-C^* transition, similar to those found for de Vries–type Sm-A^*-Sm-C_A^* transition as described earlier. These are listed in Table III.

Figure 13(a) shows the variation of the $\Delta\epsilon_s$, α, $\chi_f C_f$, and γ for increased percentages of the ferroelectric component in the mixture. We see that the soft mode strengths at the de

TABLE III. Comparison of different parameters of different compositions of MC-815 and MC-881 mixture.

Landau parameters	Mixture-1	Mixture-2	Mixture-3
$\Delta\epsilon_s$	9.8	8.8	5.5
α (kN m^{-2} rad^{-2} K^{-1})	(7.8 ± 0.4)	(33.5 ± 2.4)	(51.8 ± 2.9)
$\chi_f C_f$ (V μm^{-1} rad^{-1})	(52.3 ± 2.7)	(144.9 ± 7.8)	(153.8 ± 7.3)
γ (Pa s)	$(6 \pm 0.5) \times 10^{-3}$	$(2.6 \pm 0.2) \times 10^{-2}$	$(3.2 \pm 0.5) \times 10^{-2}$
CW regime (K)	9.5	8	7.5

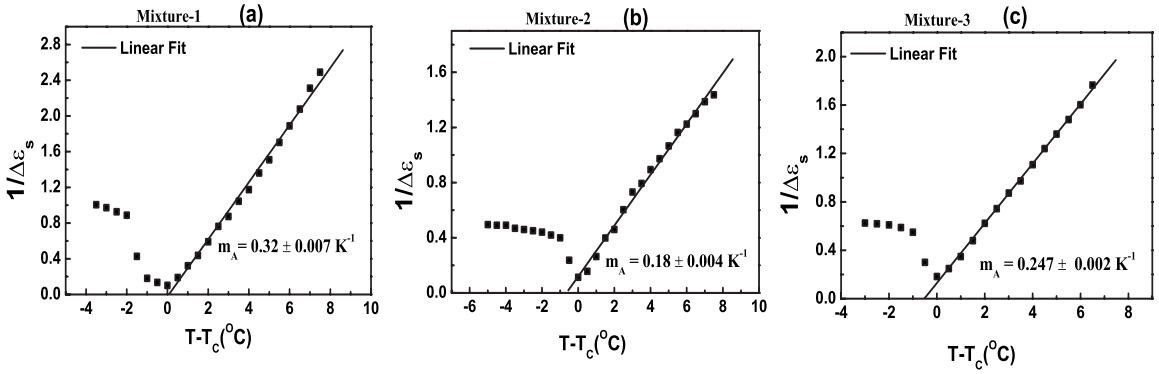

FIG. 12. Curie-Weiss plot at the de Vries–type Sm-A^*-Sm-C^* transition of (a) Mixture-1, (b) Mixture-2, and (c) Mixture-3 for 20 μm cell without application of bias field.

Vries–type Sm-A^*-Sm-C^* transition temperature are 9.8, 8.8, and 5.5 for Mixture-1, Mixture-2, and Mixture-3, respectively, which means that the soft mode strength is reduced by 10% for Mixture-2 and 44% for Mixture-3 compared to the strength of Mixture-1. Decrease in the dielectric strength of the soft mode corresponds to an increase in the ferroelectric composition at the mixture. We also note that the value of the Landau coefficient α increases with increased ferroelectric composition at the mixture. The theoretical value of the ratio of the slopes of the Sm-C^* phase and the de Vries–type Sm-A^* phase (m_{C^*}/m_{A^*}) in the Curie-Weiss plot is -2 over a certain temperature range [45], called the mean-field regime where the Curie-Weiss law is valid. The mean-field regime, also called the Curie-Weiss regime is characterized by the following [20]:

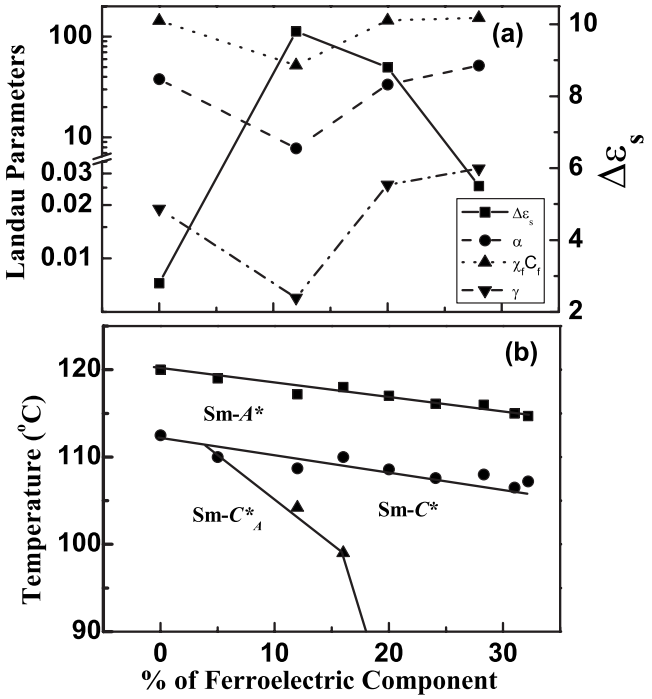

FIG. 13. (a) Variation of the soft mode dielectric strength and different Landau parameters with increased ferroelectric component in the mixtures. (b) The phase diagram of the ferroelectric and antiferroelectric liquid crystal mixture for thin cells.

$$T_c - T_o \approx \frac{3b^2}{4\alpha c}. \tag{12}$$

T_0 is the crossover temperature from the mean-field to tricritical behavior and α, b, and c are the coefficients of the Landau expansion for the free energy density as described earlier. We see that the Curie-Weiss temperature interval is slightly narrower for Mixture-3 ($\approx$7.5 K) and Mixture-2 ($\approx$8 K) compared to Mixture-1 ($\approx$9.5 K). This is in accordance with an increased ferroelectric composition of the mixture. Values of the Curie-Weiss temperature interval are calculated by subtracting the temperature up to which $1/\Delta\epsilon_s$ vs $T-T_c$ plot is linear in Sm-C^* phase up to linearity in Sm-A^* phase. Assuming that the coefficients b and c should be of the same order of magnitude for all the mixtures, according to Eq. (12), a larger value of the Landau coefficient α will lead to a narrower Curie-Weiss temperature range supported by our experimental observations. The major part of the restoring force to the tilt angle fluctuations (soft mode fluctuations) generally should be the elastic energy associated with tilt-induced changes of the smectic layer spacing. The smaller the elastic energy needed to change the director tilt and, consequently, smaller is the restoring force to the tilt-angle fluctuations. In other words, the weaker the coupling between tilt and layer spacing, the stronger the soft mode fluctuations [20]. We assume that, with increased ferroelectric composition in the mixture, the layer spacing at the de Vries–type Sm-A^*-Sm-C^* transition increases, as a result, the soft mode dielectric relaxation strength decreases, Landau coefficient α increases and the Curie-Weiss regime decreases with increased ferroelectric composition in the mixture. All the parameters of Landau expansion were found from electric-optic and dielectric studies of a ferroelectric liquid crystalline copolymer by Kocot *et al.* [47] similarly and compared with a homopolymer [48]. In particular the viscosity coefficients for the materials studied here are much smaller than found before.

The phase diagram of the studied ferroelectric and antiferroelectric liquid crystal mixture for thin cells is shown in Fig. 13(b). We see that the soft mode dielectric strength and the other related Landau parameters of the de Vries–type Sm-A^* phase exhibiting transitions to Sm-C^*_A and Sm-C^* phases are of the same order of magnitude except for the

composition where on the phase diagram the phase sequence is I-Sm-A^*-Sm-C^*-Sm-C_A^*. This may be related to the fact that the molecular fluctuations in Sm-A^* are large as both Sm-C^* and Sm-C_A^* are stable leading to large amplitude of the soft mode and this in consequence leads to a large dielectric strength and subsequently α, $\chi_f C_f$, and γ decrease. The interlayer molecular interactions in such a case could be responsible for this observation.

III. CONCLUSION

The existence of de Vries–type Sm-A^* phase in a pure AFLC compound and its mixtures with an FLC compound is confirmed by observing a change in the color of the planar texture with external electric field, and a reduction in the value of the optical birefringence with decreasing temperature within the Sm-A^* phase. It is also shown that at the transition temperature from de Vries Sm-A^* to Sm-C_A^*, the birefringence decreases because of the anticlinic alignment between the neighboring layers in the Sm-C_A^*. At the transition from de Vries–type Sm-A^* to Sm-C^* phase, the birefringence increases by approximately 12.7%, as the helical structure is suppressed by the surface anchoring in the Sm-C^* phase. The Landau parameters associated with the Sm-A^*-Sm-C_A^* transition in the pure AFLC and Sm-A^*-Sm-C^* transition in different mixtures with increased ferroelectric composition are calculated using Landau theory of the second-order phase transition from dielectric measurements. We note that the soft mode dielectric relaxation strength decreases, Landau coefficient α increases and the Curie-Weiss temperature range decreases at the de Vries–type Sm-A^*-Sm-C^* transition with increased ferroelectric composition in the mixture. These observations can be explained by assuming that, with increased ferroelectric composition in the mixture, the layer shrinkage at the de Vries–type Sm-A^*-Sm-C^* transition increases as a result of strong coupling between the tilt and the layer thickness. For low layer shrinkage materials, the restoring force of the tilt-angle fluctuations is smaller. As a result, the soft mode dielectric relaxation strength decreases, Landau coefficient α increases, and the Curie-Weiss regime decreases with increased ferroelectric composition in the mixture.

It is also found that the soft mode dielectric strength and other related Landau parameters of the de Vries–type Sm-A^* phase exhibiting transitions both to Sm-C_A^* and to Sm-C^* phases are of the same order of magnitude except where the phase sequence on the phase diagram is I-Sm-A^*-Sm-C^*-Sm-C_A^*. Measurements on mixtures close to an almost vertical line separating the phases Sm-C_A^* and Sm-C^* on the phase diagram may lead to further interesting results.

ACKNOWLEDGMENTS

We gratefully acknowledge Mitsubishi Gas Chemical Co. and Nissan Chemical Industries for donating their LC materials, MC-881 and MC-815 and the aligning agent, RN1175, respectively. We thank the Science Foundation of Ireland (SFI), Grant No. 02/In.1/I031, for funding this work. One of the authors (J.K.S.) thanks Samsung Electronics Co. for leave of absence from Seoul.

[1] R. Korlacki, A. Fukuda, and J. K. Vij, Europhys. Lett. **77**, 36004 (2007).
[2] T. P. Rieker, N. A. Clark, G. S. Smith, D. S. Parmar, E. B. Sirota, and C. R. Safinya, Phys. Rev. Lett. **59**, 2658 (1987).
[3] N. Hiji, Y. Ouchi, H. Takezoe, and A. Fukuda, Jpn. J. Appl. Phys. **27**, L1 (1988).
[4] S. T. Lagerwall, A. Dahlgren, P. Jägemalm, P. Rudquist, K. D'have, H. Pauwels, R. Dabrowski, and W. Drzewinski, Adv. Funct. Mater. **11**, 87 (2001).
[5] L. S. Matkin, S. J. Watson, H. F. Gleeson, R. Pindak, J. Pitney, P. M. Johnson, C. C. Huang, P. Barois, A.-M. Levelut, G. Srajer, J. Pollmann, J. W. Goodby, and M. Hird, Phys. Rev. E **64**, 021705 (2001).
[6] D. M. Walba, E. Korblova, L. Eshdat, M. C. Biewer, H. Yang, C. Jones, M. Nakata, M. Talarico, R. Shao, and N. A. Clark, J. Soc. Inf. Disp. **15**, 585 (2007).
[7] S. Diele, P. Brand, and H. Sackmann, Mol. Cryst. Liq. Cryst. **16**, 105 (1972).
[8] A. de Vries, Mol. Cryst. Liq. Cryst. **41**, 27 (1977).
[9] A. de Vries, J. Chem. Phys. **71**, 25 (1979).
[10] A. de Vries, A. Ekachai, and N. Spielberg, Mol. Cryst. Liq. Cryst. **49**, 143 (1979).
[11] N. Hayashi, A. Kocot, M. J. Linehan, A. Fukuda, J. K. Vij, G. Heppke, J. Naciri, S. Kawada, and S. Kondoh, Phys. Rev. E **74**, 051706 (2006).
[12] F. Giesselmann, P. Zugenmaier, I. Dierking, S. T. Lagerwall, B. Stebler, M. Kaspar, V. Hamplova, and M. Glogarova, Phys. Rev. E **60**, 598 (1999).
[13] P. J. Collings, B. R. Ratna, and R. Shashidhar, Phys. Rev. E **67**, 021705 (2003).
[14] J. P. F. Lagerwall, F. Giesselmann, and M. D. Radcliffe, Phys. Rev. E **66**, 031703 (2002).
[15] N. A. Clark, T. Bellini, R.-F. Shao, D. Coleman, S. Bardon, D. R. Link, J. E. Maclennan, X. H. Chen, M. D. Wand, D. M. Walba, P. Rudquist, and S. T. Lagerwall, Appl. Phys. Lett. **80**, 4097 (2002).
[16] F. Giesselmann, J. P. F. Lagerwall, G. Andersson, and M. D. Radcliffe, Phys. Rev. E **66**, 051704 (2002).
[17] O. E. Panarina, Yu. P. Panarin, J. K. Vij, M. S. Spector, and R. Shashidhar, Phys. Rev. E **67**, 051709 (2003).
[18] J. V. Selinger, P. J. Collings, and R. Shashidhar, Phys. Rev. E **64**, 061705 (2001).
[19] Yu. P. Panarin, F. Antonelli, O. E. Panarina, Y. Semenova, J. K. Vij, M. Reihmann, and G. Galli, Ferroelectrics **310**, 111 (2004).
[20] M. Krueger and F. Giesselmann, Phys. Rev. E **71**, 041704 (2005).
[21] M. S. Spector, P. A. Heiney, J. Naciri, B. T. Weslowski, D. B. Holt, and R. Shashidhar, Phys. Rev. E **61**, 1579 (2000).
[22] O. E. Panarina, Yu. P. Panarin, F. Antonelli, J. K. Vij, M. Reih-

mann, and G. Galli, J. Mater. Chem. **16**, 842 (2006).
[23] A. Mikulko, M. Marzec, S. Wrobel, J. Przedmojski, R. Douali, C. Legrand, R. Dabrowski, and W. Haase, Chem. Phys. Lett. **431**, 289 (2006).
[24] N. Hayashi, T. Kato, A. Fukuda, J. K. Vij, Yu. P. Panarin, J. Naciri, R. Shashidhar, S. Kawada, and S. Kondoh, Phys. Rev. E **71**, 041705 (2005).
[25] M. V. Gorkunov, F. Giesselmann, J. P. F. Lagerwall, T. J. Sluckin, and M. A. Osipov, Phys. Rev. E **75**, 060701(R) (2007).
[26] C. V. Lobo, S. K. Prasad, and D. S. Shankar Rao, Phys. Rev. E **72**, 062701 (2005).
[27] K. Saunders, D. Hernandez, S. Pearson, and J. Toner, Phys. Rev. Lett. **98**, 197801 (2007).
[28] M. Takeuchi, K. Chao, T. Ando, T. Matsumoto, A. Fukuda, and M. Yamashita, Ferroelectrics **246**, 1 (2000).
[29] Y. Yoshioka, M. Johno, T. Yui, and T. Matsumoto, European Patent No. EP1039329 (2000).
[30] J. Pavel and M. Glogarova, Liq. Cryst. **9**, 87 (1991).
[31] G. P. Crawford, R. E. Geer, J. Naciri, R. Sashidhar, and B. R. Ratna, Appl. Phys. Lett. **65**, 2937 (1994).
[32] R. E. Geer, S. J. Singer, J. V. Selinger, B. R. Ratna, and R. Shashidhar, Phys. Rev. E **57**, 3059 (1998).
[33] L. Lejček and S. Pirkl, Liq. Cryst. **8**, 871 (1990).
[34] J. Li and S.-T. Wu, J. Appl. Phys. **95**, 896 (2004).
[35] W. H. De Jeu, *Physical Properties of Liquid Crystalline Materials* (Gordon and Breach, New York, 1980).
[36] I. Muševič, R. Blinc, and B. Žekš, *The Physics of Ferroelectric and Antiferroelectric Liquid Crystals* (World Scientific, Singapore, 2000).
[37] C. C. Huang, S. T. Wang, X. F. Han, A. Cady, R. Pindak, W. Caliebe, K. Ema, K. Takekoshi, and H. Yao, Phys. Rev. E **69**, 041702 (2004).
[38] B. Žekš, Mol. Cryst. Liq. Cryst. **114**, 259 (1984).
[39] R. Blinc and B. Žekš, Phys. Rev. A **18**, 740 (1978).
[40] B. Žekš and M. Čepič, Liq. Cryst. **14**, 445 (1993).
[41] S. Sarmento, M. R. Chaves, P. S. Carvalho, and H. T. Nguyen, Liq. Cryst. **28**, 1561 (2001).
[42] K. Hiraoka, Y. Ouchi, H. Takezoe, A. Fukuda, S. Inui, S. Kawano, M. Saito, and H. Iwane, Mol. Cryst. Liq. Cryst. **199**, 197 (1991).
[43] M. Kimura, M. Yamada, and T. Akahane, Ferroelectrics **214**, 59 (1998).
[44] M. Glogarova, C. Destrade, J. P. Marcerou, J. J. Bonvent, and H. T. Nguyen, Ferroelectrics **121**, 285 (1991).
[45] F. Gouda, K. Skarp, and S. T. Lagerwall, Ferroelectrics **113**, 165 (1991).
[46] E. Gorecka, D. Pociecha, M. Glogarova, and J. Mieczkowski, Phys. Rev. Lett. **81**, 2946 (1998).
[47] A. Kocot, R. Wrzalik, J. K. Vij, M. Brehmer, and R. Zentel, Phys. Rev. B **50**, 16346 (1994).
[48] A. Kocot, R. Wrzalik, J. K. Vij, and R. Zentel, J. Appl. Phys. **75**, 728 (1994).
[49] K. Hiraoka, Y. Takanishi, K. Skarp, H. Takezoe, and A. Fukuda, Jpn. J. Appl. Phys., Part 2 **30**, L1819 (1991).